Polymer Chemistry

Accepted Manuscript

ROYAL SOCIETY OF CHEMISTRY

www.rsc.org/polymers

Polymer Chemistry

RSCPublishing

ARTICLE

Synthesis of Poly(vinylidene fluoride-*co*-bromotrifluoroethylene) and Effects of Molecular Defects on Microstructure and Dielectric Properties

Cite this: DOI: 10.1039/xoxxoooooox

Received ooth January 2012,
Accepted ooth January 2012

DOI: 10.1039/xoxxoooooox

www.rsc.org/

Matthew R. Gadinski[a], Chalatorn Chanthad[a], Kuo Han[a], Lijie Dong[b,*], Qing Wang[a,*]

A series of copolymers composed of vinylidene fluoride (VDF) and bromotrifluoroethylene (BTFE) have been synthesized via suspension polymerization up to crystallinity inhibition. P(VDF-*co*-BTFE) copolymers exhibit different regioregularity in comparison to previously reported PVDF based copolymers owing to differences in size and reactivity of BTFE. The polymerization of the comonomers result in molecular defects that are shown to be both included (single BTFE defects) and excluded (runs of BTFE monomers) from the crystalline phase. The effects of increasing defect concentrations determined by ^{19}F NMR were evaluated on the resulting microstructures by using Fourier transformed infrared spectroscopy, differential scanning calorimetry, and wide-angle X-ray diffraction. Dielectric properties have been investigated in terms of complex permittivity as a function of frequency and temperature. The results indicate that the single BTFE defects are incorporated into the crystalline phase and destabilize the ferroelectric β phase, while the excluded defects reduce both lamellar and lateral crystallite sizes though also resulting in a significant drop in crystallinity. The excluded defects are found to expand the interlamellar region of the crystalline phase, which increases both temperature and frequency dependence of the dielectric β relaxation.

Introduction

Poly(vinylidene fluoride) (PVDF) based ferroelectric polymers have been a class of electroactive materials of continued research and interest for several decades owing to the variety of technologies where this class of polymers show potential, including transducers, actuators, artificial muscles, sensors, non-volatile memory storage, capacitors, and flexible electronics.[1-3] The high dielectric constant (e.g. *K~12* @ 1 kHz) and ferroelectric properties of PVDF arise from the highly polar C-F bonds of the polymer backbone which organize into complex polymorphic crystalline phases.[2,4] The crystalline phase can then be tailored through processing or application of an electric field.

PVDF exists in four main crystalline phases designated α, β, γ, and δ. The most common and the one formed by melt crystallization is the α phase consisting of a *trans-gauche* (TG) chain conformation packed into an tetragonal unit cell.[2,4] The anti-parallel orientations of the dipoles of this phase lead to a net-zero polarization and paraelectric properties. With application of an electric field with a magnitude of 150-200 MV/m, the α phase is transformed to δ phase possessing the same crystal structure and chain conformation.[2,4] However, with dipoles oriented parallel in the unit cell, the δ phase possesses dipole moments of 1.20 and 1.02 D perpendicular and parallel to the chain axis, respectively, with the anisotropy in values arising from inclination of the dipoles.[4] With the application of electric fields of 400-450 MV/m, the α/δ phases are transformed to the β phase which can also be formed from mechanical stretching and solution casting from polar solvents.[2,4] The β phase exhibits the highest dipole moment of the PVDF polymorphs of 2.1 D resulting from an all-*trans* chain conformation.[2,4,5] The γ phase is the final PVDF polymorph comprised of a TTTG chain conformation with the same dipole moments as the δ phase. The γ phase can be formed from solution casting or annealing close to the α phase melting temperature (~160 °C).[2,4]

Besides varying processing conditions, structure modification through co- or ter-polymerization has also been demonstrated as an effective means of tailoring the crystal structures and thus the ferroelectric properties of PVDF. For example, copolymerization of VDF with trifluoroethylene (TrFE) has been found to prevent formation of the *gauche* conformation associated with the α, γ, and δ phases, allowing for direct formation of the β phase from melt solidification.[4,5] While this greatly simplifies the processing to produce ferroelectric samples, TrFE as a defects also increases the size

of ferroelectric domains and decreases dipole reversibility leading to high polarization saturation (D_{sat}~0.1 C/m^2 @ 150 MV/m) and remanent polarization (D_{rem}~0.09 C/m^2).[4,5] Tailoring the chemical composition of these copolymers has also demonstrated the ability to vary the Curie transition temperature with TrFE content.[6]

Other examples of defect modification include the incorporation of bulky comonomers into the PVDF chain in attempts to increase dipole reversibility and dielectric response at room temperature. The most successful example is the copolymerization of VDF with chlorotrifluorothylene (CTFE). In this case CTFE has been found to be included into the crystalline phase evidenced by the expansion of the lateral unit cell dimensions.[7] The increased distance between polymer chains within the crystals reduces steric hindrance to dipole motion and improves dipole response to an electric field and reversibility.[8] At sufficient CTFE content, the large size of the defect destabilizes the all-*trans* chain conformation of the β phase, allowing for the copolymers to remain in the non-polar α phase even after uniaxial stretching.[7,9] Furthermore, it has been found that this defect reduces or even removes the energy barriers for the transformation of α to β phases under applied field and enables reversible phase transformations[10], which greatly enhances the maximum polarization by preventing polarization saturation while lowering remnant polarization (<0.02 C/m^2 at ≥ 600 MV/m).[8]

Similar attempts to improve dipole reversibility have been made by copolymerizing with hexafluoropropylene (HFP). The substantially larger HFP defect prevents crystalline inclusion, and is completely excluded from the crystalline phase.[11,12] The reactivity of HFP with itself during synthesis is essentially zero, leading to randomly dispersed defects in the copolymer chain.[13] In this way the control of HFP content allows for tuning of both total crystallinity and crystallite size of the copolymers.[11] Reduction of crystallite size has also been found to improve dipole reversibility by reducing the co-operative polarization of large ferroelectric domains.[9,11]

It is clear that the tailorability of the PVDF crystalline structure and thus ferroelectric properties depends strongly on defect size and concentration.[6-11] In this paper we describe the synthesis and characterization of a series of copolymers of VDF and bromotrifluoroethylene (BTFE) with systematically increased BTFE content up to the loss of crystallinty. For the first time, the effects of BTFE content on microstructure and dielectric properties of the copolymers have been investigated. It is found through ^{19}F NMR that P(VDF-*co*-BTFE) contains regiodefects that are different than those found in previously reported PVDF based copolymers, which have significant influence on the crystalline phase and chain conformations as revealed by differential scanning calorimetry (DSC), wide angle X-ray diffraction (WAXD), and Fourier transformed infrared spectroscopy (FTIR) analysis. The effects of these structural defects on the dielectric properties of P(VDF-*co*-BTFE) were then evaluated by use of both frequency and temperature dependent dielectric spectroscopy.

Experimental

Materials

VDF and BTFE were purchased from Synquest Laboratories Inc. and purified by the freeze-thaw method. Potassium peroxodisulfate was purchased from Sigma Aldrich and used as received.

Synthesis of P(VDF-*co*-BTFE)s

The copolymers of VDF and BTFE were synthesized via a batch, suspension polymerization using a 300 mL stainless steel Parr reaction vessel. 100 mL of de-ionized water and 0.15 g potassium peroxodisulfate initiator was added to the vessel which was subsequently sealed and degassed via vacuum pump and cooled using liquid nitrogen bath. Gaseous VDF and BTFE were separately pumped into the reaction vessel at liquid nitrogen temperature using a Parr controller allowing for control of the flow rates of each monomer. Upon entering the vessel the gaseous monomers would condense and solidify. VDF was pumped in at a rate of 523.6 cm^3/min. BTFE was pumped in at a rate of 385 cm^3/min. The amount of monomer was controlled by controlling the time of each monomer that was allowed to flow into the reaction vessel. The total amount of copolymer was determined from the time, flow rate, and specific gaseous volume (listed on MSDS) at room temperature. After addition of each monomer to the vessel, vacuum was applied again before sealing the vessel and heating. The vessel was heated to 90 °C and stirred at 600 rpm for 12 hours or until the vessel pressure became stable for 2 hours. Once the reaction was complete, the polymer was washed by vacuum filtration with both distilled water and methanol, and then dried at 90 °C for 24 hours. The reactions produced typically 15-20 g of white powder polymer with a yield of 50-60%. GPC measurement using a Viscotek TDA 302 with DMF (0.01 M LiBr) as eluent running at 65 °C with a refractive index detector calibrated by universal calibration with polystyrene standards gave a $M_{n\ of}$ ~60,000 g/mol and a PDI of ~1.9.

Polymer Film Preparation

The polymer films were produced via the melt press method. The powder polymers were heated in hydraulic press to 20 °C above their respective melting temperatures. Once the desired temperature was achieved, the pressure was increased by 500 psi every 15 minutes up to 6500 psi. The films were left at pressure and temperature for a minimum of 2 hours to ensure film uniformity and maximum thinness. The films were then removed from the press and allowed to air cool at room temperature. Film thicknesses varied between 10-20 μm. The copolymer films with <2 mol % BTFE were flexible, which can be folded without cracking, and cloudy in appearance. Films with >2 mol% BTFE were increasingly brittle. Further increases in BTFE content to >3 mol% BTFE led to soft, rubbery films which were transparent. These were used in all

structural characterization and dielectric measurements. For the dielectric measurements, the polymers were sputter coated with gold using a Denton Vacuum Desk IV sputter coater under an argon atmosphere at 50 mtorr with the instrument setting of 47% power for 125 seconds. The estimated electrode thickness was 30 nm.

Characterization

^{19}F (^{1}H) NMR spectra were obtained on Bruker CDPX-300 NMR (7T, 300 MHz) using a $CFCl_3$ (TMS) internal standard. Samples were dissolved in deuterated DMSO and scanned 250 (100) times. The data was acquired using a 11.3 (12.1) μs pulse width, 1.0 (1.0) s relaxation delay, 7.4 (81.0) μs dwell time, 90° (90°) flip angle, 67567.57 (6172.84) Hz spectral window, 0.515 (0.094) Hz FID resolution, and 0.96998 (5.3085) s acquisition time. The size of processed data was 65536 which was set to half that of the total data. The spectral reference frequency was 282.13 (299.87) MHz. The spectra were processed utilizing no broadening factors and were both phase and base line corrected. DSC curves were acquired using a TA instrument model Q 100 DSC under nitrogen atmosphere and a heating/cooling rate of 10 °C/minute ramping from 20 to 200 °C for 2 cycles. The endotherms reported are of the second cycle. FTIR spectra were obtained on a Bruker V70 FTIR using an attenuated total reflectance mode with a Harrick MVP-Pro Star equipped with a diamond prism. Samples were scanned 100 times. One-dimensional XRD was performed using a PANalytical Xpert pro MPD with films analyzed in a powder geometry using a 10 mm beam mask and 0.5 inch antiscatter slit. The radiation source was a Cu Kα source with a wavelength of 1.54 Å. Peak deconvolution was done using Jade XRD analysis software using either Gaussian or Pearson VII peaks, which ever resulted in the lowest $<R^2>$ value. Crystallinity from DSC was used to guide fits. Complex dielectric constant as function of frequency at room temperature was analyzed with an Agilent E4980A LCR meter using a 2 V bias. For temperature dependent dielectric measurements, a Hewlett Packard 4284 LCR meter in conjunction with a Delta Design oven model 2300 equipped with liquid nitrogen cooling was utilized under the same bias.

Results and Discussion

Synthesis and ^{19}F NMR Analysis

BTFE as a defect is different from previously explored defect monomers such as CTFE and HFP. In terms of size, BTFE is an intermediate defect in comparison to CTFE and HFP with van der waals radii of Br, Cl, and $–CF_3$ of 185, 175, and 270 pm, respectively.[14,15] Though larger than CTFE, BTFE is significantly smaller than HFP and should still be capable of inclusion in the crystalline phase, offering further expansion of the unit cell dimensions in comparison to CTFE. In addition, BTFE exhibits a different reactivity ratio when polymerized with VDF. Copolymerization of CTFE and HFP with VDF forms random copolymers with primarily single defects dispersed throughout the chain, resulting from reactivity ratios for P(VDF-*co*-CTFE) of r_{VDF}=0.73 and r_{CTFE}=0.75 (at 80 °C) (ref. 16) and for P(VDF-*co*-HFP) of r_{VDF}=3 and r_{HFP}=0 (at 85 °C) (ref. 13). Other brominated comonomers such a 1-bromo-2,2-difluroethylene (BDFE) have also been reported in copolymerization with VDF. Similar to P(VDF-*co*-CTFE)s and P(VDF-*co*-HFP)s, however, the reported reactivity ratios for P(VDF-*co*-BDFE) are r_{VDF}=1.2 and r_{BDFE}=0.4 (at 75 °C) indicating a higher reactivity of VDF.[17]

In comparison, P(VDF-*co*-BTFE) exhibits reactivity ratios of r_{VDF}=0.43 and r_{BTFE}=1.46 (at 80 °C) (ref. 16). As a consequence, the BTFE radical on the growing copolymer chain shall link more significantly with the defect monomer in the reaction mixture than either P(VDF-*co*-CTFE) or P(VDF-*co*-HFP). In this way P(VDF-*co*-BTFE)s shall contain two separate types of molecular defects being singular BTFE monomers and runs of multiple BTFE monomers, which have different effects on the crystallinity and microstructure.

Synthesis of P(VDF-*co*-BTFE)s was carried out by suspension polymerization with the chemical composition varied by controlling the initial monomer concentrations. This was done by controlling flow rates and times of the monomers as listed in Table 1.

The copolymer compositions listed in Table 1 were determined utilizing Equation 1[16]:

Table 1. Copolymerization conditions and polymer compositions

Sample	Monomer Flow Time [a]		Moles of Monomer		Monomer Feed Fraction		Copolymer Composition (mol%)[b]	
	VDF (min)	BTFE (s)	VDF	BTFE	VDF	BTFE	VDF	BTFE
PVDF	17.5	0	0.378	0.0	1.0	0.0	100	0
PVB1	18.5	7	0.400	0.002	0.995	0.005	99.5	0.5
PVB2	17.5	10	0.378	0.003	0.992	0.008	99.3	0.7
PVB3	17.5	25	0.378	0.007	0.982	0.018	98.0	2.0
PVB4	17.5	45	0.378	0.012	0.969	0.031	97.2	2.8
PVB5	17.5	90	0.378	0.024	0.940	0.060	95.4	4.6
PVB6	17.5	120	0.378	0.032	0.922	0.078	94.7	5.3
PVB7	17.5	157	0.378	0.042	0.900	0.100	91.3	8.7

[a] monomer flow rates listed in experimental section
[b] calculated from ^{19}F NMR spectra and Equation 1

$$\frac{\text{mol \% VDF}}{\text{mol \% BTFE}} = \frac{I_1 + I_2 + 3I_3 - I_4}{I_5 + I_6 + 2(I_4 - I_3)} \bullet \frac{3}{2} \quad (1)$$

The representative ^{19}F NMR spectra of P(VDF-*co*-BTFE)s are presented in Figure 1a. Values $I_{1\text{-}6}$ of Equation 1 correspond to the integration of peaks within the ppm ranges[19] listed in Table 2. The calculated compositions are found to match the initial monomer concentrations reasonably well with increasing deviation at higher BTFE concentrations.

The reason for this deviation is attributed to chain transfer reaction evidenced by the peaks at -46.49, -48.50, -63.80, and -166.23 ppm which are assigned to $-CH_2CF_2CH_2C\underline{\boldsymbol{F}}_2Br$, $-CF_2CH_2CH_2C\underline{\boldsymbol{F}}_2Br$, $-CH_2CF_2CH_2CF_2C\underline{\boldsymbol{F}}_2Br$, and alkyl fluorine species, respectively.[13,20-22] These reactions result from the labile nature of C-Br bond often targeted as crosslinking sites in fluoropolymers.[13,17]

Besides, as a consequence of this weak C-Br bond, a degree of branching is possible due to Br cleavage, which likely results in the alkyl fluorine peak occurring at -166.23 ppm. Evidence of branching and chain transfer can also be seen in the ^{1}H NMR spectrum of **PVB7** (Figure S1) which shows peaks for brominated end groups (2.6 ppm) and hydrogen terminated end groups (6.5 ppm).[21] To characterize this branching the intensity of the alkyl fluorine peak is compared with the intensity of those resulting from brominated end groups of the ^{19}F spectra to estimate the number of brominated end groups that result from bromine cleavage of the copolymer chain. It was found for **PVB7** with the highest BTFE content in both the polymer and reaction feed only 30% of the brominated end groups could be a result of bromine cleavage from the main chain, indicating that the chain transfer reactions are occurring primarily with the BTFE monomer during synthesis.

Also listed in Table 2 are the five carbon sequences associated with the peaks between -90.0 and -140.0 ppm originating from the $-CF_2-$ groups and their local linkages.[24] This region is highlighted in Figure 1b which also labels the spectral ranges. These sequences are determined through comparison of the ^{19}F spectra of P(VDF-*co*-BTFE) with that of P(VDF-*co*-CTFE). These copolymers exhibit the same peaks between -90 and -140 ppm, which are assumed to arise from the same sequences except for the difference of a single atom on the defect monomer being a Cl to a Br, for P(VDF-*co*-CTFE)

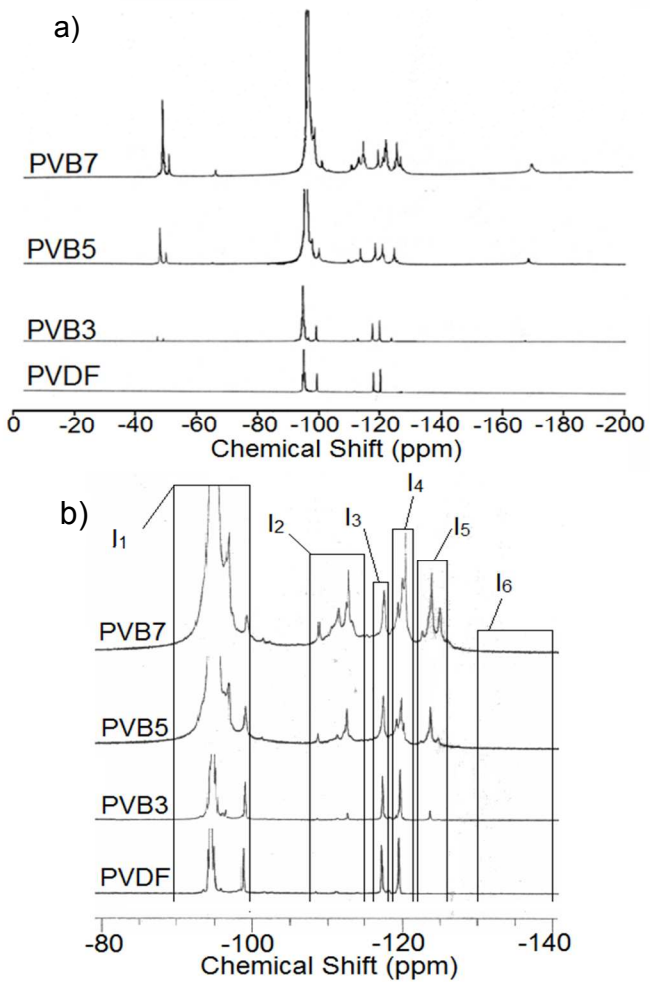

Figure 1. a) ^{19}F NMR spectra of selected copolymers with increasing BTFE content at a reference frequency of 282 MHz in deuterated DMSO at room temperature with shifts relative to a $CFCl_3$ standard. b) ^{19}F Spectra with increasing BTFE content between -80 and -140 ppm ($I_{1\text{-}6}$ corresponds to spectral ranges of Table 2)

Table 2. Spectral ranges of Equation 1 and associated five carbon sequences and designations.

Spectral Range [b]	Sequence [b]	Designation (H (head)-CF_2, T (tail)- CH_2, CFBr)	Chemical Shift (ppm)
I_1	$-(CF_2CH_2)-(C\underline{\boldsymbol{F}}_2CH_2)-CF_2-$	VDF-VDF (T-H) VDF-VDF (T-H)[a]	-94.36
	$-CFBr-(CH_2C\underline{\boldsymbol{F}}_2)-(CH_2CF_2)-$	BTFE-VDF (T-T) VDF-VDF (H-T)	-95.16 to -95.67
	$-CH_2-(CH_2C\underline{\boldsymbol{F}}_2)-(CH_2CF_2)-$	VDF-VDF (T-T) VDF-VDF (H-T)	-96.26 to -99.13
I_2	$-CF_2-(CFBrC\underline{\boldsymbol{F}}_2)-(CFBrCF_2)-$	VDF-BTFE (H-T)[a] BTFE-BTFE (H-T)	-108.05 to -109.82
	$-CF_2-(CH_2C\underline{\boldsymbol{F}}_2)-(CF_2CFBr)-$	VDF-VDF (H-T)[a] VDF-BTFE (H-H)	-110.0 to -111.34
	$-(CF_2CFBr)-(C\underline{\boldsymbol{F}}_2CFBr)-CH_2-$	BTFE-BTFE (T-H) BTFE-VDF (T-T)	-111.34 to -115.10
I_3	$-CF_2-(CH_2C\underline{\boldsymbol{F}}_2)-(CF_2CH_2)-$	VDF-VDF (H-T)[a] VDF-VDF (H-H)	-116.27
I_4	$-(CH_2CF_2)-(C\underline{\boldsymbol{F}}_2CH_2)-CH_2-$	VDF-VDF (H-H) VDF-VDF (T-T)	-118.57
I_5	$-(CH_2CF_2)-(C\underline{\boldsymbol{F}}_2CFBr)-CH_2-$	VDF-BTFE (H-H) BTFE-VDF (T-T)	-120.25 to -121.98
	$-CF_2-(CF_2C\underline{\boldsymbol{F}}Br)-(CH_2CF_2)-$	VDF-BTFE (H-H)[a] BTFE-VDF (T-T)	-122.35 to -125.32
I_6	$-(CF_2CH_2)-(C\underline{\boldsymbol{F}}BrCF_2)-CH_2-$	VDF-BTFE (T-T) BTFE-VDF (H-T)	-131.46 to -132.53
	$-CH_2-(CF_2C\underline{\boldsymbol{F}}Br)-(CF_2CH_2)-$	VDF-BTFE (T-H) BTFE-VDF (T-H)	-138.57 to -139.17

[a] if the final carbon was a head unit, the monomer could not be identified and was assumed to be VDF as it dominated all copolymer compositions. [b] corresponds to $I_{1\text{-}6}$ of Equation 1.[18,19]

and P(VDF-*co*-BTFE), respectively. Due to the low concentration of defect monomer in the copolymer, peaks of spectral range I_6 never develop.

From these sequences the regioregularity and monomer linking tendencies were determined through comparison of the integrated peak areas and the designations of Table 2.[25] For the homo-polymerization of VDF, the monomers tend to link H-T (head to tail) with T-T and H-H linkages being regiodefects in the chain structure which affects crystallinity,[26] which are presented in Figure 2a. The copolymer contains additional defect linkages which ultimately determine the microstructure of the polymer. The percentages of the linkage defects across the composition range are summarized in Figure 2b with the remainder of the percentage at each composition attributable to VDF-VDF (H-T) linkages.

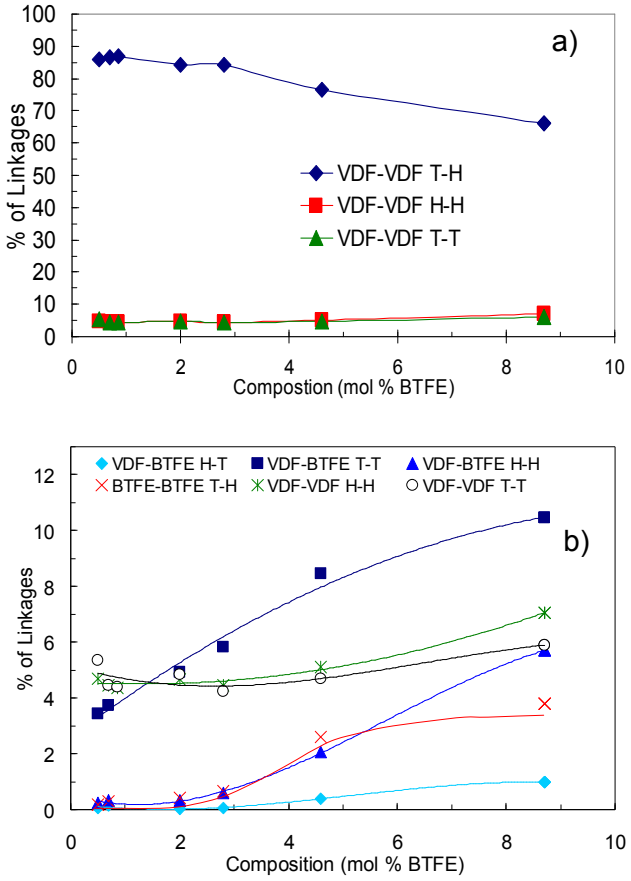

Figure 2. a) Distribution of VDF-VDF containing linkages as a function of composition b) Percentage of defect linkages present in the copolymer chains as a function of BTFE content (H-head (CF_2), T-tail (CH_2, CFBr). Analysis is non-directional meaning linkages such as VDF-VDF (T-H) were taken as equivalent to VDF-VDF (H-T)).

VDF-VDF (H-T) is the dominant linkage at all compositions varying from 86% to 66% for 0.5 to 8.7 mol% BTFE, respectively (seen in supporting information, Figure S3). This value begins to drop considerably for the compositions above 2 mol% BTFE with corresponding increases in the defect percentages. As VDF-VDF H-H regiodefects are normally followed by a T-T addition, these defect linkages are found in similar amounts across the composition range.[26] The VDF-VDF regiodefects are also seen to increase with BTFE content, indicating that the addition of the BTFE monomer increases the regioirregularity of the chain, as a defective VDF addition likely follows the addition of any BTFE monomer.

The primary BTFE containing linkage is found to be the VDF-BTFE (T-T) which becomes the dominant linkage defect above 2 mol% BTFE. Similarly, for P(VDF-*co*-CTFE)s the linkages are dominated by VDF-VDF (H-T) and VDF-CTFE (T-T) linkages.[19] However, above 2 mol% BTFE the BTFE-BTFE (T-H) linkages are more significant than the CTFE-CTFE (T-H) linkage in P(VDF-*co*-CTFE)s as expected from the reactivity ratio difference. For 8.7 mol% BTFE, the BTFE-BTFE T-H linkage percentage is comparable to a literature report for a P(VDF-*co*-CTFE) copolymer containing 18.8 mol% CTFE.[19]

To estimate the number of BTFE monomers per run, we first assume that the polymers have a number average molecular weight of 60,000 g/mol (from GPC-see Experimental Section). From the polymer molecular weight and weight average (from composition) molecular weight of both monomer units, the degree of polymerization is estimated to be ~910. The chain being composed of 910 monomer units equates to 909 linkages per chain. As seen from Figure 2, 0.41% of these linkages correspond to BTFE-BTFE (T-H) linkages. This indicates ~4 such linkages per chain, assuming that one run of BTFE monomers would be comprised of 5 BTFE monomers. For the P(VDF-*co*-BTFE) with 8.7 mol% BTFE, following the same assumptions, the total number of BTFE-BTFE T-H linkages would be 38, meaning that there would be ~10 runs of BTFE monomers of equal size to the singular run in the P(VDF-*co*-BTFE) with 2 mol% BTFE. It is assumed for P(VDF-*co*-CTFE) and extended to this polymer that there is at least a partial inclusion of singular, halogenated defects into the crystalline phase as evidenced by unit cell expansion and *β* phase destabilization.[7,9,10] However, where single defects are expected to be included, the growth of large blocks of BTFE defects are anticipated to be excluded and reduce crystallizable length of the polymer chain. These effects are observed in P(VDF-*co*-BTFE)s and discussed below.

Chain Conformation Studied by FTIR

FTIR was utilized to analyze the effect of the increasing defect concentration on the chain conformations present in the copolymers. As mentioned in the introduction, TrFE with similar size to the VDF monomer stabilizes the ferroelectric phase by preventing the *gauche* conformation associated with all other crystalline phases of PVDF.[5,6] Larger defects in comparison induce twists into the polymer chain i.e. *gauche* conformation to accommodate the bulky comonomers and stabilize the non-polar phase.[7,8] In both cases the composition of the defect monomer strongly affects the conformations

present. Figure 3 shows the FTIR spectra from 400-1600 cm^{-1} of the copolymers with increasing BTFE content.

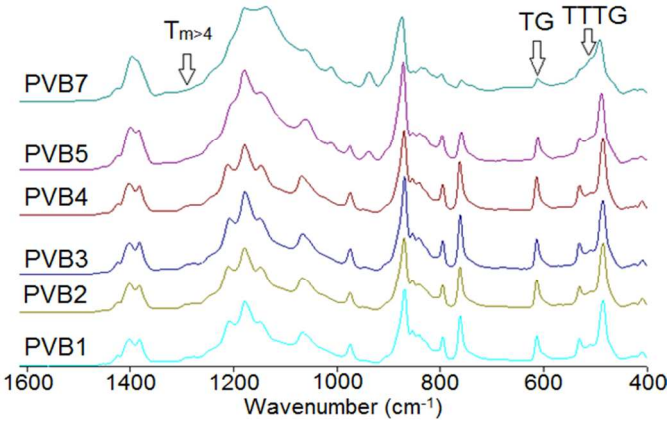

Figure 3. FTIR spectra of P(VDF-*co*-BTFE)s with increasing BTFE content from 400-1600 cm^{-1} (T-trans conformation, G-gauche conformation)

Of interest are the peaks located at 505, 614, and 1290 cm^{-1} corresponding to TTTG, TG, and all-*trans* conformations, respectively. These chain conformations are characteristic of those found in the γ, α, and β crystalline phases.[27] Figure 4 shows the fractions of these conformations present in the copolymer films as a function of composition calculated from the ratio of peak absorbance.[19]

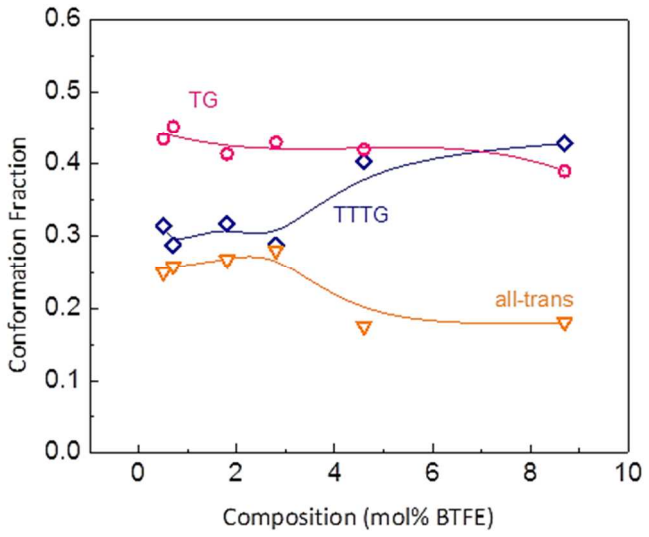

Figure 4. Conformation fractions of TTTG, TG, and all-*trans* (T-trans, G-gauche) chain conformations as a function of composition.

The TG conformations are found to vary little with composition, comprising 40-45% of the conformations with a slight decrease towards higher compositions. This indicates that the α phase is the dominant crystalline phase across the composition range.[27] Initially, the TTTG and all-*trans* conformations are present in similar amounts. This changes above 2 mol% BTFE as the values for the TTTG and all-*trans* conformation diverge with the TTTG being found in similar amounts to the TG with the all-*trans* decreasing in the opposite fashion.

The change in conformation corresponds to the increasing BTFE concentration and increasing defect linkages of the polymer chain. Specifically, the composition where the increase in the TTTG conformation is observed, corresponds to the same composition where the VDF-BTFE T-T became the dominant linkage defect (Figure 2) and the regioregular VDF-VDF T-H linkage begins to drop predictably (see Supporting Information). These results confirm that BTFE does introduce the *gauche* conformation and breaks up all-*trans* sections into smaller blocks of TTTG sections. This further suggests the destabilization of the β phase at 4.5 mol% BTFE which is not seen in P(VDF-*co*-CTFE)s until 9 mol% CTFE.[7]

Unfortunately, there appears to be no literature reports available which discuss the chain conformation distribution of other PVDF copolymers, *i.e.* P(VDF-*co*-CTFE)s, P(VDF-*co*-HFP)s, P(VDF-*co*-TrFE)s, as a function of defect monomer content, so no direct comparison with P(VDF-*co*-BTFE) copolymers shown in Figure 4 could be made. However, the more random nature of the copolymerization in P(VDF-*co*-CTFE)s and P(VDF-*co*-HFP)s may lead to a more subtle changes with composition than the abrupt changes observed in P(VDF-*co*-BTFE)s.

Crystalline Phase Characterization

FTIR can only provide relative changes of the crystalline phase as a consequence of peaks being attributable to conformations existing in a particular crystalline phase, cannot be discerned from those present in the amorphous phase. Also, FTIR is incapable of differentiating the respective effects of the differing BTFE defects on crystalline dimensions. DSC and WAXD were thus employed to directly probe the effects on the crystalline phase. DSC was utilized to characterize the crystalline phase in terms of melting temperature and total crystallinity with the results shown in Figure 5 (melting

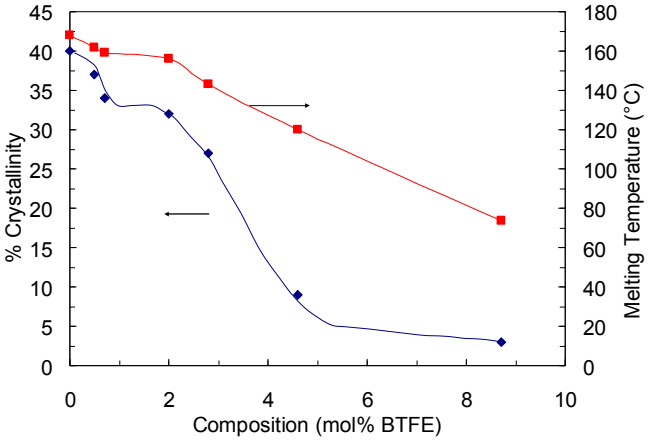

Figure 5. Melting temperature and crystallinity as a function of composition determined from DSC (crystallinity determined from $\Delta H_f^{o,\,PVDF}$= 104.7 J/g).[28]

endotherms shown in Figure S2 of Supporting Information).

This plot reveals the melting temperatures and total crystallinity are fairly stable up to 2 mol% BTFE with the small initial drops likely due to incorporation of BTFE defects into the crystalline phase.[29] The massive drop in both these values occurring above 2 mol% BTFE, however, cannot be explained by defect inclusion, and therefore must arise from defect exclusion.[29]

The changes in these values correspond to the sudden increase in the BTFE-BTFE T-H linkage as seen in Figure 2 and the development of blocks of BTFE defect monomers which cannot be accommodated in the crystalline phase. This is also evidenced by the increasing broadness of the melting endotherms with BTFE content, indicating increasing heterogeneity of composition as a consequence of the variable number of BTFE segments in a block and their spacing on the polymer chain.[30] The growth of these blocks and their exclusion causes a decrease in lamellar thickness limited by the chain lengths between these blocks indicated by the drop in melting temperature related to lamellar thickness through the Gibbs-Thompson equation.[31]

In comparison, P(VDF-*co*-CTFE) with 9 mol% CTFE is greater than 20% crystalline and maintains 7.5% crystallinity even at 25 mol% CTFE.[8,31] However, even P(VDF-*co*-HFP) with 4 mol% HFP possess >30% crystallinity with melting temperatures >140 °C (refs.11, 12), indicating a difference in the nature of the defect exclusion in P(VDF-*co*-BTFE)s. To elucidate the discrepancy in crystallinity, WAXD was utilized to further characterize the crystalline phase and crystalline dimensions.

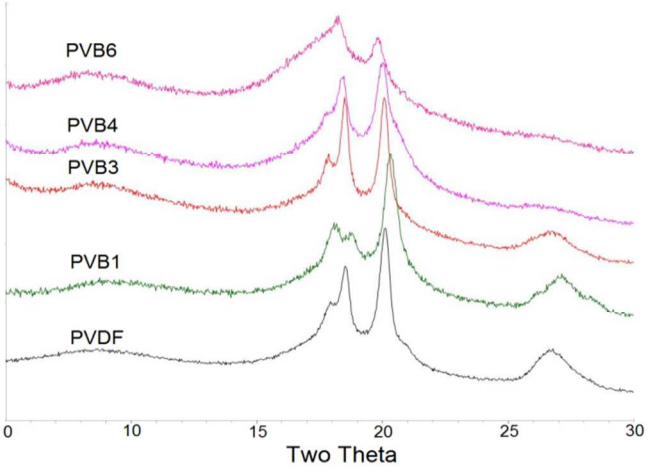

Figure 6. WAXD spectra of P(VDF-*co*-BTFE) copolymers with increasing BTFE content between 0° to 30° 2θ.

Figure 6 shows the WAXD spectra of P(VDF-*co*-BTFE)s with increasing BTFE content. The presence of at least two phases is confirmed by the XRD spectra which exhibit α phase peaks located at 17.66°, 18.30°, 19.90°, and 26.56° 2θ related to the (100), (020), (110), and (021) planes, respectively, and the presence of a shoulder off the 19.90° peak corresponding to the (110/200) plane of the β phase.[27] The presence of the γ phase is difficult to determine from XRD due to the similarity of its unit cell with that of the α phase and possessing almost identical characteristic peaks, along with fact that at least some α phase is invariably present in any samples containing γ phase.[27,33] However, the sudden jump in the 18.30° 2θ peak seen in **PVB3** may be an indication of its formation, which is supported by the increase in the TTTG conformation from the FTIR results.

Figure 7 compares the phase distributions as determined from the fits to the WAXD spectra. Indicated by the continual absorption of the crystalline peaks into the amorphous halo seen in Figure 6, the substantial drop in crystallinity observed in DSC is corroborated with a 20% increase in the amorphous content between 2 and 5 mol% BTFE. The α phase is confirmed to be the dominant crystalline phase, dropping continuously with BTFE content. The β phase content is found to initially be fairly stable up to ~3 mol% BTFE, but quickly drops to zero slightly above 5 mol% BTFE. These results are consistent to the relative trends found in the chain conformation distributions determined by FTIR.

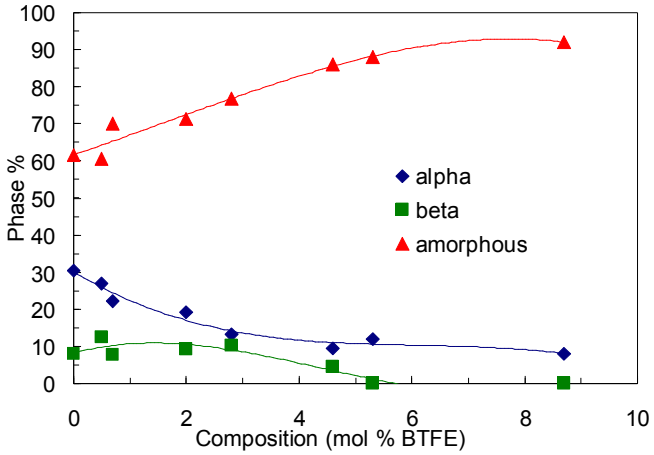

Figure 7. Content of crystalline and amorphous phases determined from fits WAXD spectra with increasing BTFE content.

The inclusion of the BTFE defect is evidenced by the shift in peaks to lower 2θ seen in Figure 6 corresponding to increases in the D-spacing related by Bragg's Law, which is also observed in P(VDF-*co*-CTFE)s.[7] Figure 8 shows the calculated D-spacings for the lateral unit cell dimensions. Both the lattice spacings for the (100) and (020) planes of the α phase are found to increase with increasing BTFE content, indicating increased inclusion of the defect. The larger size of the defect with respect to CTFE is also displayed with P(VDF-*co*-CTFE)s, exhibiting a lattice spacing of 5.2 Å at a composition of >25 mol% CTFE (ref. 27) comparable to that of the 8.7 mol% BTFE composition of P(VDF-*co*-BTFE)s.

Also, of note in Figure 8 is the expansion of the lattice spacing associated with the (110/200) plane of the β phase, indicating a degree of defect inclusion into this phase prior to destabilization. Inclusion of the defect into the β phase is expected for TrFE (refs. 5 and 6), but has not been previously

reported for bulky comonomers. Though from these results it is likely also present to some degree in P(VDF-*co*-CTFE).

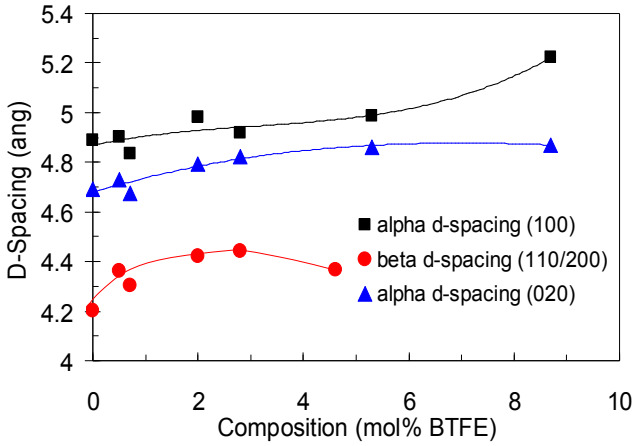

Figure 8. D-Spacing of lateral crystalline planes of α and β phases as a function of BTFE content.

Further understanding of the nature of the excluded defects can be found by looking to the trends in the lateral crystallite sizes calculated from the Scherrer equation shown in Figure 9. Seen in Figure 9 are the crystallite sizes for (100) and (020) *α* phase, in which crystallite sizes initially increase in the region where only included defects are present. This is expected for included defects and also observed in the homo-polymer with increasing HHTT defects.[26] However, as the excluded defect concentration begins to increase, the crystallite size drops dramatically from >250 Å at 2 mol% BTFE to <90 Å at 8.7 mol% BTFE. This large drop in crystallite size is likely linked to the considerable decrease in crystallinity with relatively small amount of defect concentration.

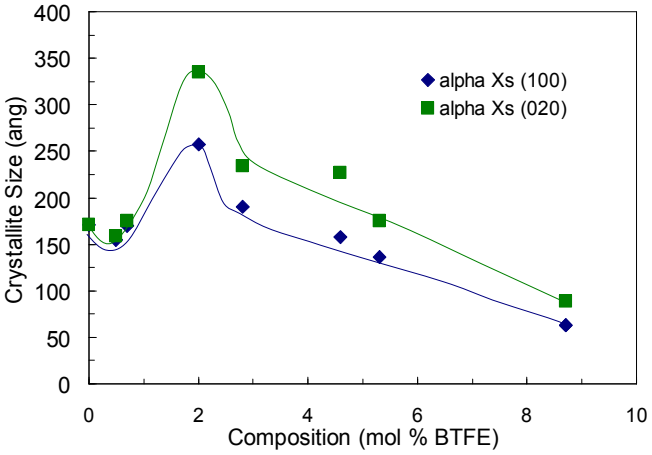

Figure 9. Crystallite size of lateral planes of the *α* phase crystals calculated from the Scherrer equation.

Unlike lamellar thickness which is dependent on the amount and spacing of excluded defects, the lateral crystallite size is only dependent on the availability of polymer chains with suitable crystallizable length able to be added to the growing lamella.[30] In P(VDF-*co*-HFP)s, HFP is found as isolated excluded defects randomly dispersed in the polymer chain. With the excluded defects being constituted by only a single monomer unit, the remaining P(VDF-*co*-HFP) chain has a larger chance of adding to another growing lamella or reinserting into the same lamella than would be case in P(VDF-*co*-BTFE)s. The multiple monomer excluded defect of P(VDF-*co*-BTFE)s would be forced to loop farther into the interphase region between lamella and limit re-insertion, while any additional defect BTFE blocks on the dangling chain would further inhibit its ability to add to another local growing lamella. In this way P(VDF-*co*-HFP)s are able to maintain its crystallinity to higher HFP contents than P(VDF-*co*-BTFE)s at comparable compositions. This results in the interphase region of P(VDF-*co*-BTFE)s to be increasingly populated by dangling amorphous chains, which is evident in the dielectric spectroscopy.

Dielectric Characterization

Figure 10 contains the frequency dependent dielectric spectroscopy of P(VDF-*co*-BTFE)s with increasing BTFE content. All P(VDF-*co*-BTFE) copolymers show increased permittivity over PVDF. The copolymer values vary between 10.6 and 11.3 compared to 9 for PVDF at 1 kHz. The increase in permittivity is attributed to the expanded unit cell dimension which improves dipole response to an electric field.[4]

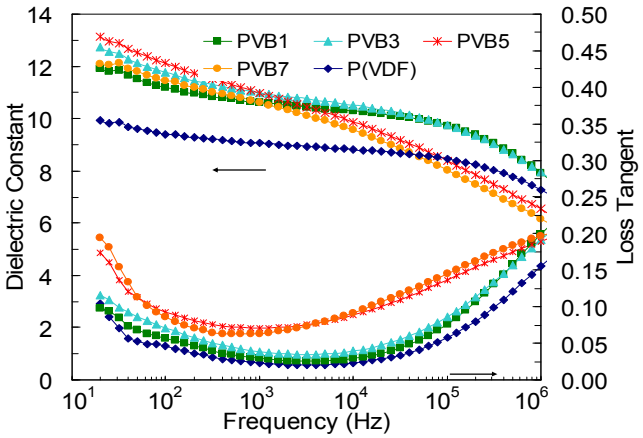

Figure 10. Frequency dependent room-temperature dielectric spectroscopy of the copolymers with increasing BTFE content.

However, it is seen for samples with compositions of 4.6 mol% BTFE and higher (**PVB5**, **PVB7**) that there exists increasing frequency dependence of permittivity which drops off rapidly above 1 kHz. This is contrary to the plateau behavior observed in PVDF and lower BTFE content copolymers. The reason for this change in frequency dependence can be found by looking to the loss tangent curves. At low frequencies (under 100 Hz) the loss tangent is seen to increase with decreasing crystallinity, consistent with increasing conduction loss resulting from increased chain mobility.[34] As frequency increases, copolymers **PVB5** and **PVB7** exhibit an increase in the loss tangent at 1 kHz which not

observed in lower BTFE composition samples until 100 kHz. To further probe this relaxation, temperature dependent dielectric spectroscopy has been performed with the loss tangent results for **PVB1** and **PVB6** with varying frequencies shown in Figure 11.

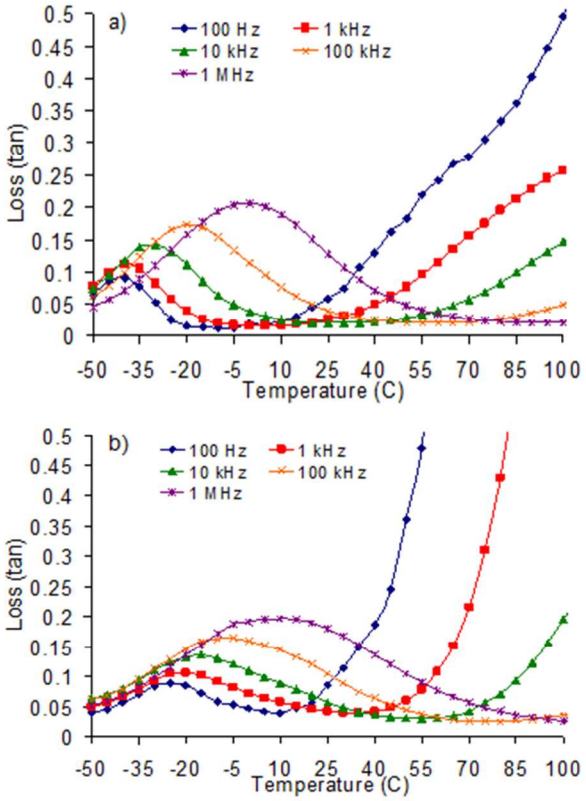

Figure 11. Temperature dependent loss tangent of a) **PVB1** and b) **PVB6** at various frequencies.

The broad relaxation occurring between -40 °C and about room temperature in both samples is denoted as the β or α_a relaxation depending on reference.[35-38] This relaxation is attributed to the manifestation of the dynamic glass transition (T_g) of the amorphous phase.[35-38] With increasing BTFE content, the peak shifts to higher temperature as T_g increases with BTFE content from -40° C for PVDF to -18 °C for **PVB6** determined from DSC. While shifting to higher temperature, the peaks are also observed to decrease in intensity and broaden at comparable frequencies. The behavior of this peak differs from the composition dependence of P(VDF-*co*-HFP)s where the peak is found to increase in intensity and become sharper with increasing amorphous content.[39-41] Generally speaking, purely amorphous polymers which exhibit such a relaxation should appear fairly sharp resulting from the isotropic nature of the amorphous phase[40] with micro-brownian motions, whereas this peak is attributed to due to its Vogel-Fulcher-Tammann dependence[35-38], becoming active over a relatively small window. For **PVB6** this relaxation begins to broaden into the room temperature regime, while for **PVB1** this does not occur until 100 kHz, which is consistent with the room temperature frequency dependent results.

To explain these discrepancies the expanding interphase must be considered. As the amorphous content of these copolymers increases with BTFE content, a larger portion of this amorphous phase must be located at the interphase instead of existing as free amorphous chains. Due to the inherently bound nature of the interphase at a given frequency, the peak broadens preferentially to higher temperature to accommodate. Similar behavior has also been observed in miscible blends of poly(methylmethacrylate) (PMMA) and PVDF.[43,44] As PMMA content is increased in these blends, the β relaxation is observed to decrease in value while also broadening. This has been attributed to PMMA, while being miscible with PVDF, does not co-crystallize, and as a result inhibits chain re-insertion and expands the interphase.[43-44]

Conclusions

A series of copolymers composed of VDF and BTFE were synthesized to determine the effect of the presence of included and excluded defects into the chain structure of VDF. For small amounts of BTFE (<2 mol%), the comonomer is dispersed primarily as single defects and minimally affect crystallinity and chain conformation distributions. As BTFE content is further increased and the prevalence of BTFE monomer runs increases, there is found to be a substantial drop in crystallinity and crystallite size along with the inhibiting of the all-*trans* chain conformation shortly followed by the destabilization of the ferroelectric β phase. Dielectrically it is found that, at sufficiently high defect concentration, the room temperature permittivity becomes linear on log scale with frequency, which is attributed to the increasing frequency dependence of the β relaxation resulting from the glass transition of the amorphous phase. The β relaxation is found to decrease in value while also broadening with increasing BTFE content in the temperature dependent dielectric spectroscopy, contradicting the expected change with increasing amorphous content and those observed in P(VDF-*co*-HFP)s with increasing HFP content. The changes in the β relaxation do, however, mirror the effects observed in blends of PVDF and PMMA attributed to the segregation of PMMA to the surface of PVDF crystals, resulting in an expansion of the interphase between lamellar crystallites. Similarly, the large size of the excluded defects in P(VDF-*co*-BTFE)s are also asserted to expand this interphase, evidenced by the broad melting endotherms and reduction of the lateral crystallite sizes along with the temperature dependent dielectric spectroscopy.

In many proposed applications of PVDF based copolymers, such as in high energy density capacitors or for piezoelectric applications, high crystallinity is desired for the best performance. In this regard, P(VDF-*co*-BTFE) copolymers would be limited to low BTFE concentrations due to the deleterious effect of the long runs of BTFE monomers. However, with the insight of the effect of these long runs on crystallinity, synthesis strategies can be employed in attempts to reduce their prevalence. This also has implications for

P(VDF-*co*-CTFE)s where the drop in crystallinity is one of primary limitations of this class of copolymers.

The low crystallinity samples on the other hand still exhibit impressive permittivity values for a polymeric material, which would also be benefitted from the improved solubility through crystallinity reduction. As PVDF inherently exhibits poor solubility and has limited number of good solvent, this added solution processability could find use in areas such as thin film transistors where solution processing is preferred. The high amount of weak C-Br bonds in these copolymers also would allow for facile chemical crosslinking which can improve dielectric performance via reduction of conduction losses and improved breakdown strength.[45]

Acknowledgements

This work was supported by Dow Chemical Company and National Natural Science Foundation of China (No. 51373132).

Notes and references

[a] Department of Material Science and Engineering, The Pennsylvania State University, University Park, Pennsylvania 16802 (USA). E-mail: wang@matse.psu.edu

[b] State Key Laboratory of Advanced Technology for Materials Synthesis and Processing, and School of Materials Science and Engineering, Wuhan University of Technology, Wuhan 430070, People's Republic of China. E-mail: dong@whut.edu.cn

† Electronic Supplementary Information (ESI) available: [^{1}H NMR spectrum of PVB7 and melting endotherms of selected copolymer samples]. See DOI: 10.1039/b000000x/

1 H. S. Nalwa, in *Ferroelectric Polymers*, ed. Marcel Dekker, New York, 1st edn., 1995, vol. 1, ch. 2, pp. 80-85.
2 A. J. Lovinger, *Science,*1983, **220**, 1115-1121.
3 J. M. Herbert, T. T. Wand, A. M. Glass. in: *The Application of Ferroelectric Polymers,* ed. Chapman and Hall, London, 1st edn., 1998, pp. 37-42.
4 L. Zhu, Q. Wang, *Macromolecules,* 2012, **45**, 2937-2954.
5 T. Furukawa, *Adv. Colloid Interface Sci.,* 1997, **71-72**, 183-208.
6 Y. Tajitsu, A. Chiba, T. Furukawa, M. Date, E. Fukada, *Appl. Phys. Lett.,* 1980, **36**, 286-288.
7 B. Chu, X. Zhou, K. Ren, B. Neese, M. Lin, Q. Wang, F. Bauer, Q. M. Zhang, *Science,* 2006, **313**, 334-336.
8 X. Zhou, B. Chu, B. Neese, M. Lin, Q. M. Zhang, *IEEE Trans. Diel. Elect. Ins.,* 2007, **14**, 1133-1138.
9 Y. Wang, X. Zhou, Q. Chen, B. Chu, Q. M. Zhang, *IEEE Trans. Diel. Elect. Ins.,* 2010, **17**, 1036-1042.
10 V. Ranjan, L. Yu, *Phys. Rev. Lett.,* 2007, **99**, 047801-1, 047801-4.
11 F. Guan, J. Wang, J. Pan, Q. Wang, Q, L. Zhu, *Macromolecules,* 2010, **43**, 6739-6748.
12 F. Guan, J. Pan, J. Wang, Q. Wang, L. Zhu, *Macromolecules,* 2010, **43**, 384-392.
13 B. Ameduri, *Chem. Rev.,* 2009, **109**, 6632-6686.
14 A. Bondi, *J. of Phys. Chem.,* 1964, **68**, 441-451.
15 J. Pflaum, G. Bracco, F. Schreiber, R. Colorado, O.E. Shmakova, T. R. Lee, G. Scoles, A. Kahn, *Surf. Sci.,* 2002, **498**, 89-104.
16 G. Moggi, P. Bonardelli, *J. of Polym. Sci.,* 1984, **22**, 357-365.
17 G. K. Kostov, L. Sauguet, B. Ameduri, H. Kaspar, T. Zipplies, K. Hintzer, *J. Polym. Sci., Part A, Polym. Chem.*, 2010, **48**, 3964-3976.
18 Y. M. Murasheva, A.S. Shaskov, F. A. Galil-Ogly, *Polymer Science U.S.S.R.,* 1980, **21**, 968-974.
19 Y. Lu, J. Claude, Q. Zhang, Q. Wang, *Macromolecules,* 2006, **39**, 6962-6968.
20 W. R. Dolbier, in *Guide to Fluorine NMR for Organic Chemists,* ed. John Wiley and Sons, Hoboken, 1st ed., 2009, ch. 2, pp. 14.
21 M. Pianca, E. Barchiesi, G. Esposto, S. Radice, *J. of Fluor. Chem.,* 1999, **95**, 71-84.
22 M. Duc, B. Ameduri, G. David, B. Boutevin, *J. of Fluor. Chem.,* 2007, **128**, 144-149.
23 A. Taguet, B. Ameduri, B. Boutevin, *Adv. Polym. Sci.,* 2005, **184**, 127-211.
24 J. Guiot, B. Ameduri, B. Boutevin, *Macromolecules,* 2002, **35**, 8694-8707.
25 T. Yagi, M. Tatemoto, *Polym. J.,* 1979, **11**, 429-436.
26 A. J. Lovinger, D. D. Davis, R. E. Cais, J. M. Kometani, *Polymer,* 1987, **28**, 617-626.
27 R. Gregorio, *J. of Appl. Polym. Sci.,* 2006, **100**, 3272-3279.
28 K. Nakagawa, Y. Ishida, *J. of Polym. Sci.; Polym. Phys. Ed.,* 1973, **11**, 2153-2171.
29 J. Wendling, U. W. Suter, *Macromolecules,* 1998, **31**, 2516-2520.
30 P. Flory, *Trans. Faraday Soc.,* 1955, **51**, 848-857.
31 P. C. Painter, M. M. Coleman, in *Fundamentals of Polymer Science*, ed. CRC Press, Boca Raton, 1st ed., 1997, ch. 8, pp. 283-285.
32 Y. Lu, J. Claude, L. E. Norena-Franco, Q. Wang, *Phys. Chem. B.,* 2008, **112**, 10411-10416.
33 A. J. Lovinger, *Polymer,* 1980, **21**, 1317-1322.
34 F. Guan, L. Yang, J. Wang, B. Guan, K. Han, Q. Wang, L. Zhu, *Adv. Funct. Mater.,* 2011, **21**, 3176-3188.
35 S. Yano, *J. of Polym. Sci.: Part A-2,* 1970, **8**, 1057-1072.
36 H. Kakutani, *J. of Polym. Sci.: Part A-2,* 1970, **8**, 1177-1186.
37 V. J. McBrierty, D. C. Douglass, T. A. Weber, *J. of Polym. Sci.,* 1976, **14,** 1271-1286.
38 H. Sasabe, S. Saito, M. Asahina, H. Kakutani, *J. of Polym. Sci.: Part A-2,* 1969, **7**, 1405-1414.
39 N. Koizumi, K. Tsunashima, S. Yano, *Polym. Lett.,* 1969, **7**, 815-820.
40 P. Frübing, F. Wang, M. Wegener, *Appl. Phys. A,* 2012, **107**, 603-611.
41 V. V. Kochervinskii, I. A. Malyshkina, G. V. Markin, N. D. Gavrilova, N. P. Bessonova, *J. of Appl. Polym. Sci.,* 2007, **105**, 1101-1117.
42 R. H. Boyd, *Polymer,* 1985, **26**, 1123-1133.
43 J. W. Sy, J. Mijovic, *Macromolecules,* 2000, **33**, 933-946.
44 B. Hahn, J. Wendorff, *Macromolecules,* 1985, **18**, 718-721.

45 P. Khanchaitit,K. Han, M. R. Gadinski, Q. Li, Q. Wang, *Nat. Commun.* 2013, **4**, 2845 (doi:10.1038/ncomms3845)